Journal of Orthopaedic Research
9:918–931 Raven Press, Ltd., New York

Computational Methods for Analyzing the Structure of Cancellous Bone in Planar Sections

Arthur D. Kuo and Dennis R. Carter

Department of Mechanical Engineering, Stanford University, Stanford; and Veterans Affairs Rehabilitation R&D Center, Palo Alto, California, U.S.A.

Summary: Conventional stereologic methods for expressing the orientation of anisotropic materials are limited to materials assumed to possess orthogonal directions of orientation. In many substances, including cancellous bone, this assumption is unsubstantiated. Presented here are two simple methods for characterizing the orientation of any anisotropic material within a plane. By modeling the substance as a series of lines oriented in particular directions, it is possible to arrive at either a "phase distribution" that expresses the degree of orientation distributed over a range of angles or a series of "primary orientations" that express the degree of orientation at a select number of angles, with an additional measure of the degree of isotropy. This characterization of anisotropy is highly dependent on such parameters as feature size, sample size, test line spacing, and test line width. Given the careful selection of these parameters, the new methods provide simple measures of orientation, which may prove useful in testing Wolff's trajectorial theory of the relationship between mechanical stresses and the orientation of cancellous bone. **Key Words:** Cancellous bone—Stereology—Wolff's law—Trajectorial theory.

Considerable attention has been paid to characterizing the orientation of cancellous bone. Much of this interest has been directed toward verifying or refuting the trajectorial theory developed by the German anatomist Wolff (26), which postulates that cancellous bone remodels to adapt to its stress environment: the trabeculae become aligned to the (mutually perpendicular) principal stress trajectories so that bone provides maximum strength with minimal weight (16). This concept evolved from the discovery by the anatomist Meyer (15) that the trabecular architecture of the femoral head resembles the principal stress trajectories in a crane drawn by the engineer Culmann. Wolff used this observation as evidence of an unspecified mathematical relationship between trabecular trajectories and applied stresses. As Roesler (20) points out in his review paper, this theory has led to a debate, consisting mostly of unsubstantiated arguments, that has remained unresolved for a number of decades. Researchers in the field of stereology have recently made more quantitative analyses of bone architecture. Whitehouse and Dyson (25) used stereologic techniques to characterize the trabeculae of the proximal human femur, including in their study a measure of the trabecular "departure from isotropy." Raux and associates (19) developed rigorous procedures for preparing specimens for stereologic analysis and applied them in a study of the trabecular architecture of the human patella. They identified zones of single or mixed orientation within the patella that suggest a sheet-and-rod

Received December 5, 1989; accepted March 12, 1991.
Address correspondence and reprint requests to Dr. A. D. Kuo at Design Division, Mechanical Engineering Department, Stanford University, Stanford, CA 94305, U.S.A.

model of the trabecular structure. Hayes and Snyder (11) extended these techniques in a rigorous quantitative comparison between trabecular architecture and principal stresses calculated from a finite element model of the patella. Providing the first quantitative support for the trajectorial theory, their findings showed a significant correlation between the orientation of the trabeculae and the computed principal stresses.

Harrigan and Mann (9) used the stereologic measure of anisotropy in orthotropic materials to form a tensor, thus consolidating orientation information in three dimensions. Cowin (4,5) used a variation of this tensor, the fabric tensor, in his mathematical formulation of Wolff's law of trabecular architecture.

The trajectorial theory as stated by Wolff has, however, also been challenged. Oxnard and Yang (17), in their study of Fourier transforms of radiographs of human and primate vertebrae, review several objections to the theory and offer modifications to Wolff's law, suggesting that cancellous bone architecture is not necessarily orthotropic (as principal stresses are). Bacon and colleagues (1) used neutron diffraction techniques to assess the orientation of trabeculae in the bones of the human foot; they showed that in areas of the calcaneus subjected to complex time-varying stresses, the trabeculae may have widely varied and sometimes nonorthotropic orientations. They also offered a revised version of Thompson's (21) diagram of the trabecular pattern in the foot, showing lines that are clearly not orthotropic. Cheal and co-workers (3) conducted a careful experiment to test the remodeling response of cancellous bone around implants in the equine patella. Their control specimens showed a significant correlation between trabecular orientation and principal stress directions calculated using a finite element model. However, they found a poor correlation between the *changes* in these two measures in their experimental patellae. Fyhrie and Carter (7) proposed a quantitative unifying principle relating stresses in bone and trabecular morphology. Applying this principle in a finite element analysis of simple loading conditions from a single direction, trabecular architecture should be orthotropic, coinciding with principal stress trajectories. However, under complex time-varying loading conditions, Carter and collaborators (2) suggest that the trabeculae should be aligned so as to best support stresses from a variety of directions (equivalent stresses), and therefore need not be orthotropic.

Stereologic studies of cancellous bone have in the past been based primarily on polar plots of the mean intercept length (*MIL*), as described below. When characterizing the orientation of a material, the plot of the *MIL* is fit to a single ellipse. Because the principal axes of an ellipse are orthogonal, this technique presupposes that the material being studied is orthotropic. This condition must be verified when applied to cancellous bone, in light of the objections to the trajectorial theory discussed above. This article describes computational methods similar to those cited by others (12,13,18), which can be used in stereologic analysis of a two-dimensional section of a substance to test for orthotropy within the plane, to give a measure of the isotropy or departure from isotropy that is superior to conventional measures, to provide quantitative evidence of the number and degree of orientations, and to test models of the material architecture directly—all of which are readily applicable to developing a better understanding of the relationship between mechanical loading and cancellous bone architecture.

CONVENTIONAL STEREOLOGY

Stereology uses statistical measures gathered from two-dimensional sections of a substance to infer information concerning the structure of the material. Underwood's (22) classic text explains in detail the stereologic technique most often used for analysis of cancellous bone morphology, the directed secant method. This method calls for laying a grid of parallel lines, at an angle Θ about an arbitrary axis, across the section, as in Fig. 1A, and counting the intersections between the test lines and the boundaries of the "trabeculae." This process is repeated with the test lines arranged at a series of angles Θ from 0 to 180°.

The total number of intersections per unit test line length $[I_L(\Theta)]$ is recorded for each angle, and its polar plot is often referred to as the "rose of intercepts," as shown in Fig. 1B. Alternatively, the inverse of $I_L(\Theta)$, the mean intercept length $MIL(\Theta)$ is plotted. Typically, a single ellipse is fit to the polar plot of $MIL(\Theta)$ (24). However, because an ellipse has orthogonal principal axes, using these axes to characterize the material orientation may be misleading if the substance is not orthotropic, even if the ellipse provides a good fit.

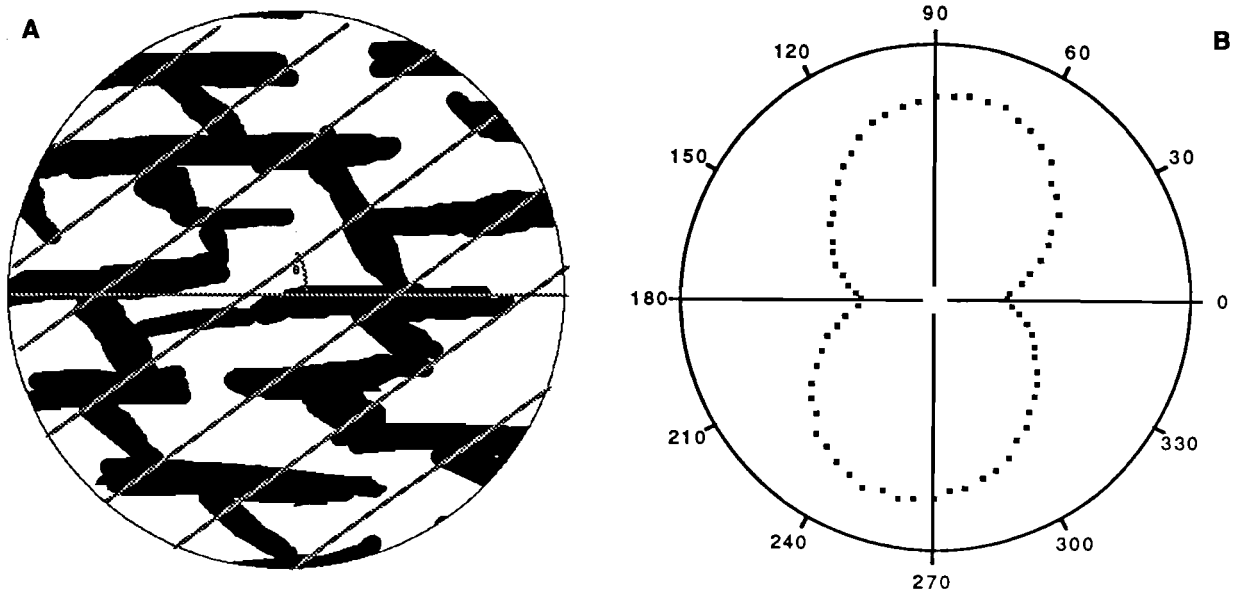

FIG. 1. A: Sample pattern exhibiting obvious nonorthotropic characteristics. Test lines at angle Θ shown. **B:** Rose of intercepts for sample pattern.

The degree of orientation is another important stereological measure. It is easily determined based on the stereological measure of the boundary length per unit area B_A (also referred to as perimeter length density). Hayes and Snyder (11) and Whitehouse and Dyson (23) used

$$B_A = \frac{\pi}{2}\overline{I_L(\Theta)} \quad (1)$$

B_A is used to find the degree of orientation

$$\%\ \text{orientation} = \frac{100[I_L(\max) - I_L(\min)]}{B_A} \quad (2)$$

This measure is most applicable for materials possessing a single direction of orientation; for materials with multiple directions of orientation, the results suggest little about the actual morphology of the test substance. For example, for the test pattern shown in Fig. 1A, which is highly oriented in two directions. Eq. 2 yields 55% orientation, which is an uninformative description.

As discussed above, trabecular bone is a complex, anisotropic material that may not possess mutually perpendicular directions of orientation. Conventional techniques of fitting an ellipse to $MIL(\Theta)$ are not adequate for describing the orientation of such a material. We will present methods based on the work of Hilliard (12) that are better suited for planar sections.

METHODS

It has been noted that the directed secant method, when applied to a sample pattern of straight lines with orientation ϕ with respect to the horizontal, will produce a rose of intercepts such as shown in Fig. 2 (22). Mathematically, the rose of intercepts for this sample pattern can be expressed as

$$I_L(\Theta) = c_0|\sin(\Theta - \phi)| \quad (3)$$

where c_0 is an indicator of the total line length in the direction ϕ. Figure 3 shows that the rose of intercepts for a sample pattern consisting of an array of straight lines in two different directions ϕ_1 and ϕ_2 is of the form

$$I_L(\Theta) = c_1|\sin(\Theta - \phi_1)| + c_2|\sin(\Theta - \phi_2)| \quad (4)$$

and c_1 and c_2 describe the relative total line lengths in the two principal directions (22). The corresponding $MIL(\Theta)$ plot is a combination of two ellipses.

Cancellous bone is often considered to be made up of struts and plates arranged in a variety of positions and directions. If we assume that a two-dimensional slice of cancellous bone exposes these structural elements as a series of lines of various lengths arranged at various positions and orienta-

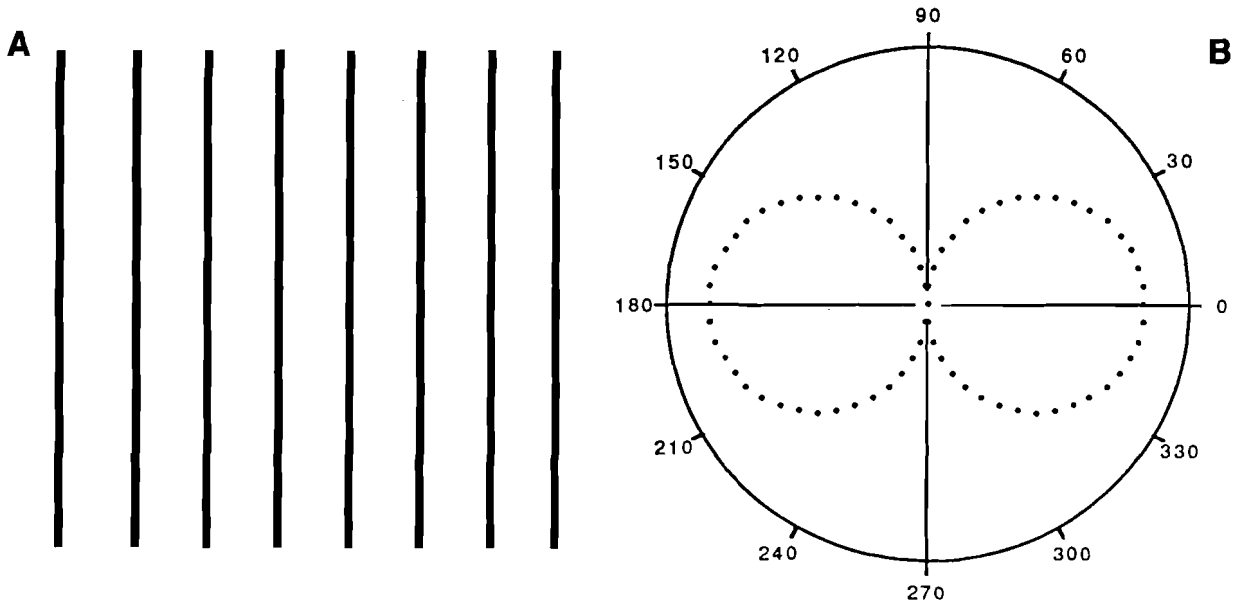

FIG. 2. A: Sample pattern of straight lines with orientation $\phi = 90°$. **B:** Corresponding rose of intercepts.

tions, we can find the estimated rose of intercepts $\hat{I}_L(\Theta)$ with

$$\hat{I}_L(\Theta) = \sum_{j=1}^{n} c_j \mid \sin(\Theta - \phi_j) \mid \qquad (5)$$

where the bone pattern is modeled as a series of lines pointing in n directions, with a weighting (or degree of orientation) c_j corresponding to each direction ϕ_j. Hilliard likened this relation to a convolution between the sine function and c expressed in the continuous domain (12).

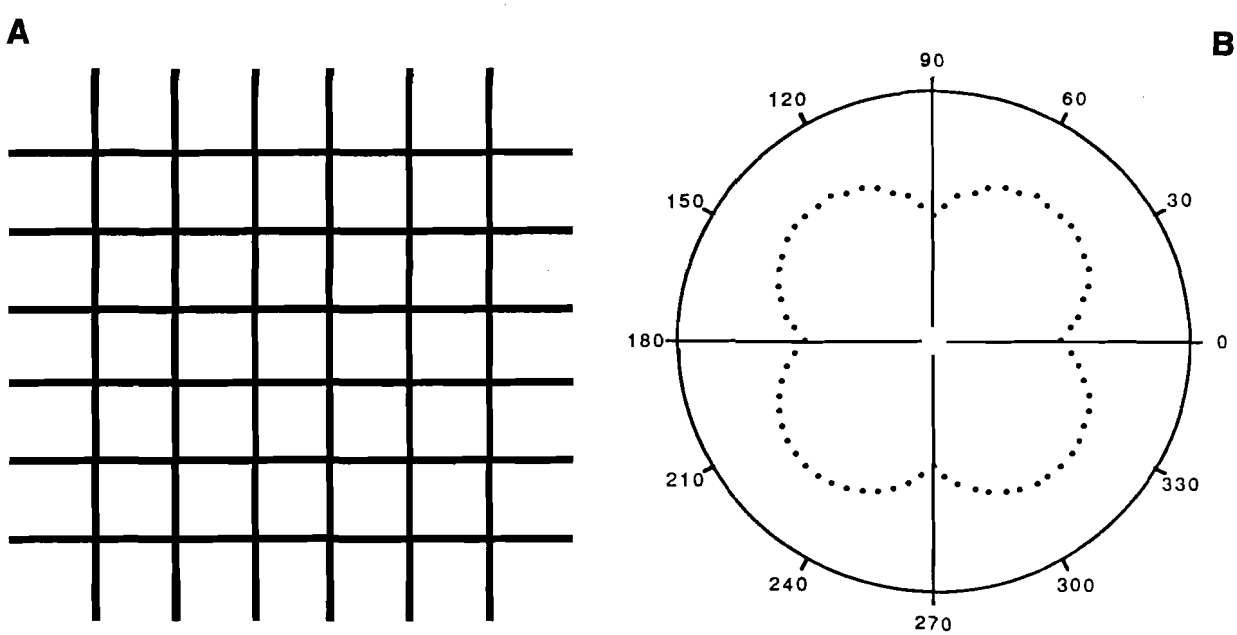

FIG. 3. A: Sample pattern of straight lines in two perpendicular directions. **B:** Corresponding rose of intercepts.

Phase Distribution Method

From Eq. 5, we see that the rose of intercepts is simply a sum of rectified sine waves of identical frequencies but varying phases—the phases being the angles of orientation. Just as a frequency distribution plot produced from a Fourier transform provides the magnitude of sinusoidal signals over a range of frequencies, the phase distribution plot provides the magnitudes of sine waves over a range of phases.

Plots similar to the phase distribution have proved useful in describing the preferred orientations of cancellous bone, but they typically are vaguely qualitative in nature (17). The rose of intercepts, however, can be used to produce a more quantitative phase distribution computationally. The technique is very flexible and is compatible with many conventional automated stereology systems.

For Hilliard (12) the continuous function c is solved by deconvolving the continuous version of Eq. 5. Unfortunately, this technique does not constrain the magnitudes to be positive, resulting in a different interpretation of c from that given above. Kanatani (13) solved the continuous problem for c [which was denoted the distribution density $f(\Theta)$] constrained positive, with a Fourier series approximation. The results are problematic for complex materials, because the harmonics of the Fourier series confuse the results. For the purposes of studying cancellous bone, we prefer discrete "bins" for the phase distribution.

To produce the phase distribution from the rose of intercepts, the angles $\phi_j (j = 1,2, \ldots, n)$ are typically selected over a range $0° \leq \phi_j < 180°$, distributed uniformly. Least-squares parameter estimation facilitates the calculation of the unknown magnitudes c_j $(j = 1,2, \ldots, n)$. If the rose of intercepts is given at m angles $\Theta_i (i = 1,2, \ldots, m)$, the number of phases that can be solved for is $n \leq m$. Use of $n \geq m$ results in overfitting of the data.

We wish to minimize the difference J between the measured rose of intercepts and that obtained from the model. Using a least-squares measure of this difference, the objective (14) can be written as

$$\text{minimize } J = \sum_{i=1}^{m} \left(I_L(\Theta_i) - \hat{I}_L(\Theta_i) \right)^2 = \sum_{i=1}^{m} \left(I_L(\Theta_i) - \sum_{j=1}^{n} c_j \left| \sin (\Theta_i - \phi_j) \right| \right)^2 \tag{6}$$

subject to $c_j \geq 0$ for $j = 1,2, \ldots, n$. This can be expanded after substituting

$$\Phi_{ij} = \left| \sin (\Theta_i - \phi_j) \right| \tag{7}$$

so that the objective is to minimize

$$J = \sum_{i=1}^{m} \left(I_L(\Theta_i)^2 + \sum_{j=1}^{n} (c_j \Phi_{ij})^2 + 2 \sum_{j=1}^{n} \sum_{k=1}^{n} c_j c_k \Phi_{ij} \Phi_{ik} - 2 I_L(\Theta_i) \sum_{j=1}^{n} c_j \Phi_{ij} \right) \tag{8}$$

subject to $c_j \geq 0$ for $j = 1, \ldots, n$. $I_L(\Theta_i)^2$ is not a function of c_j and therefore may be dropped from the objective function. By also making the following substitutions into the elements of $\mathbf{Q}$, an n by n matrix, and $\mathbf{b}$ and $\mathbf{x}$, both n by 1 vectors:

$$Q_{jk} = \sum_{i=1}^{m} \Phi_{ij} \Phi_{ik} \tag{9}$$

$$b_j = - \sum_{i=1}^{n} I_L(\Theta_i)\, \Phi_{ij} \tag{10}$$

$$x_j = c_j \tag{11}$$

for $j = 1, \ldots, n$ and $k = 1, \ldots, n$, the optimization problem may be written as

$$\text{minimize } \overline{J} = \frac{1}{2} \mathbf{x}^{\mathrm{T}} \mathbf{Q} \mathbf{x} + \mathbf{b}^{\mathrm{T}} \mathbf{x} \qquad \text{subject to } \mathbf{x} \geq \mathbf{0}. \tag{12}$$

Parameters describing the accuracy of the least-squares fit can be obtained using the following equations (6):

error sum of squares

$$SSE = \sum_{i=1}^{m} (I_L(\Theta_i) - \hat{I}_L(\Theta_i))^2 \tag{13a}$$

total sum of squares

$$SST = \sum_{i=1}^{m} (I_L(\Theta_i) - \overline{I_L(\Theta_i)})^2 \tag{13b}$$

estimated variance

$$s^2 = \frac{SSE}{n-2} \tag{13c}$$

coefficient of determination

$$r^2 = 1 - \frac{SSE}{SST} \tag{13d}$$

Primary Direction Method

The trajectorial theory as expressed by Wolff (26) argues that in a two-dimensional slice there are only two directions, intersecting at 90°, that the trabecular architecture will follow. In studying this theory, it may be desirable to compare stresses calculated with a finite element model to the two (or more) primary directions of the observed trabeculae. Once an assumption has been made concerning the number of trabecular trajectories, one can use the primary direction method to calculate the primary directions, the degree of orientation in each of the primary directions, and the degree of isotropy (the lack of orientation). While no additional information is supplied, the results are packaged in a form suitable for comparison with such models.

Suppose a test substance is known to be oriented along two directions, i.e., the substance can be modeled as straight lines at two angles $\phi_j (j = 1,2)$. These angles and the corresponding magnitudes c_j can be solved directly. Then the objective can be written as

minimize $J =$

$$\sum_{i=1}^{m} (I_L(\Theta_i) - c_1 \mid \sin(\Theta_i - \phi_1) \mid - c_2 \mid \sin(\Theta_i - \phi_2) \mid)^2 \tag{14}$$

with respect to $0° \leq \phi_j < 180°$, $c_j \geq 0$ for $j = 1,2$, which will give the best fit for two directions of orientation. Note that the difference with the phase distribution method is that ϕ_j are here considered to be unknowns.

The primary direction method described can be extended to accommodate isotropy. The rose of intercepts for a completely isotropic substance is given by

$$I_L(\Theta_i) = c_0 \quad (i = 1,2, \ldots, m). \tag{15}$$

Thus a substance with two directions of orientation and a degree of isotropy can be modeled with an estimated rose of intercepts

$$\hat{I}_L(\Theta) = c_0 + c_1 \mid \sin(\Theta - \phi_1) \mid + c_2 \mid \sin(\Theta - \phi_2) \mid \tag{16}$$

and the objective function is

minimize $J =$

$$\sum_{i=1}^{m} (I_L(\Theta_i) - c_0 - c_1 \mid \sin(\Theta_i - \phi_1) \mid - c_2 \mid \sin(\Theta_i - \phi_2) \mid)^2 \tag{17}$$

with respect to $0° \leq \phi_1 < 180°$, $0° \leq \phi_2 < 180°$, $c_0 \geq 0$, $c_1 \geq 0$, $c_2 \geq 0$.

Because this objective function is not smoothly differentiated with respect to the independent variables ϕ_j, the solution is difficult to obtain using standard nonlinear programming techniques. However, if the number of primary directions is small, search methods for ϕ_j are adequate.

A crude but simple search method is simply to use the quadratic programming technique to minimize

$J(\phi_1, \phi_2) =$

$$\sum_{i=1}^{m} (I_L(\Theta_i) - c_0 - c_1 \Phi_{i1} - c_2 \Phi_{i2})^2 \tag{18}$$

with respect to $c_0 \geq 0$, $c_1 \geq 0$, $c_2 \geq 0$ for a list of values of ϕ_1 and ϕ_2. From the table of values of $J(\phi_1,\phi_2)$, one can choose the minimum, which is the best fit for the parameters c_0, c_1, c_2, ϕ_1, ϕ_2.

To solve Eq. 18, the same technique as presented for the phase distribution method is used, except with

$$\mathbf{Q} = \begin{bmatrix} 1 & \sum_{i=1}^{m} \Phi_{i1} & \sum_{i=1}^{m} \Phi_{i2} \\ \sum_{i=1}^{m} \Phi_{i1} & \sum_{i=1}^{m} \Phi_{i1}^2 & \sum_{i=1}^{m} \Phi_{i1}\Phi_{i2} \\ \sum_{i=1}^{m} \Phi_{i2} & \sum_{i=1}^{m} \Phi_{i1}\Phi_{i2} & \sum_{i=1}^{m} \Phi_{i2}^2 \end{bmatrix} \tag{19a}$$

and

$$\mathbf{b} = \left[-\sum_{i=1}^{m} I_L(\Theta_i) \quad -\sum_{i=1}^{m} I_L(\Theta_i)\,\Phi_{i1} \quad -\sum_{i=1}^{m} I_L(\Theta_i)\,\Phi_{i2} \right]^T \tag{19b}$$

Eq. 13 can be used to calculate the coefficient of determination for the least-squares fit.

Eq. 2 is adapted so that the relative degrees of orientation and isotropy can be expressed as the relative contribution each direction makes to the total rose plot:

degree of isotropy

$$d_0 = \frac{\int_0^{\pi} c_0 d\Theta}{A} = \frac{c_0 \pi}{A} \tag{20a}$$

degree of orientation direction ϕ_1

$$d(\phi_1) = \frac{\int_0^{\pi} c_1 \mid \sin(\Theta - \phi_1) \mid d\Theta}{A} = \frac{2c_1}{A} \tag{20b}$$

degree of orientation direction ϕ_2

$$d(\phi_2) = \frac{\int_0^{\pi} c_2 \mid \sin(\Theta - \phi_2) \mid d\Theta}{A} = \frac{2c_2}{A} \tag{20c}$$

where

$$A = \int_0^{\pi} c_0 + c_1 \mid \sin(\Theta - \phi_1) \mid + c_2 \mid \sin(\Theta - \phi_2) \mid d\Theta = \pi c_0 + 2c_1 + 2c_2 \tag{20d}$$

APPLICATIONS

Phase Distribution Method

The phase distribution plot for the sample pattern in Fig. 1A is compared with the distribution density using the method of Kanatani (13) in Fig. 4. The harmonics of the distribution density make it difficult to infer orientation information from the plot. The phase distribution was produced by digitizing the image and using the directed secant method with the quadratic programming package QPSOL (8) to solve for the magnitudes c_j, all on a Macintosh II computer. The surveyed section of the sample pattern has a radius of ~250 pixels. Test lines were laid 7 pixels apart, with each test line 3 pixels wide (as described below). The test lines were rotated by computer in 5° increments. In Fig. 4, note the peaks clustered around 0° and 135°, which can easily be seen as primary directions of orientation for the test pattern. For this pattern, $r^2 = 0.9997$.

Primary Direction Method

The primary direction method was also applied to the sample pattern of Fig. 1A, using a list of all combinations of ϕ_1 and ϕ_2 for values between 0° and 175° inclusive, in 5° increments, in a search method in conjunction with QPSOL. The results are shown in Table 1, along with the results derived from the conventional method of fitting an ellipse to *MIL*(Θ) and using Eq. 2. The primary direction method produces a better match with the obvious characteristics of the sample pattern, indicating that there are "trabeculae" oriented at 0° and 135°, as opposed to the conventional elliptic *MIL* approach, which calculates principal orientations at ~−6° and 84° (by necessity, orthogonal directions). Note that the *MIL* approach produces an excellent fit ($r^2 = 0.98$) for an ellipse, even though the material is clearly not orthotropic. The primary direction method can be generalized for any number of directions, and as long as n is small, the search technique's lack of efficiency is not a limiting factor.

Finally, the two methods are applied to the same sagittal section of the second lumbar vertebra in man studied by Oxnard and Yang (17), shown in Fig. 5A. In their power spectrum of this section, Oxnard and Yang found elements at about 60° to the horizontal. The phase distribution in Fig. 5B and the results of the primary direction method for two directions in Table 2, confirm their finding. The greatest degree of orientation is at 90°, but the next most significant orientation is at 60°. The primary direction method shows that this second line of orientation is not strong (4.3%), but, more important, it demonstrates that the vertebra is not strongly orthotropic. Together with the degree of isotropy, the curve fit is quite close with $r^2 = 0.98$. In contrast, the conventional *MIL* method produces a close fit to an ellipse, but shows only that the section implies orthotropy with an orientation of 36%.

PRACTICAL CONSIDERATIONS

The methods described and applied here are highly dependent on the accuracy and resolution of the imaging systems used to digitize the image and produce the rose of intercepts. Many conventional techniques for performing automated stereology have inherent inaccuracy associated with the digitization of the sample image. This is true of computer analysis systems that either rotate test lines at varying angles across a stationary sample or lay a constant set of test lines across a sample that is rotated within the computer memory.

Image analysis inaccuracies are difficult to detect

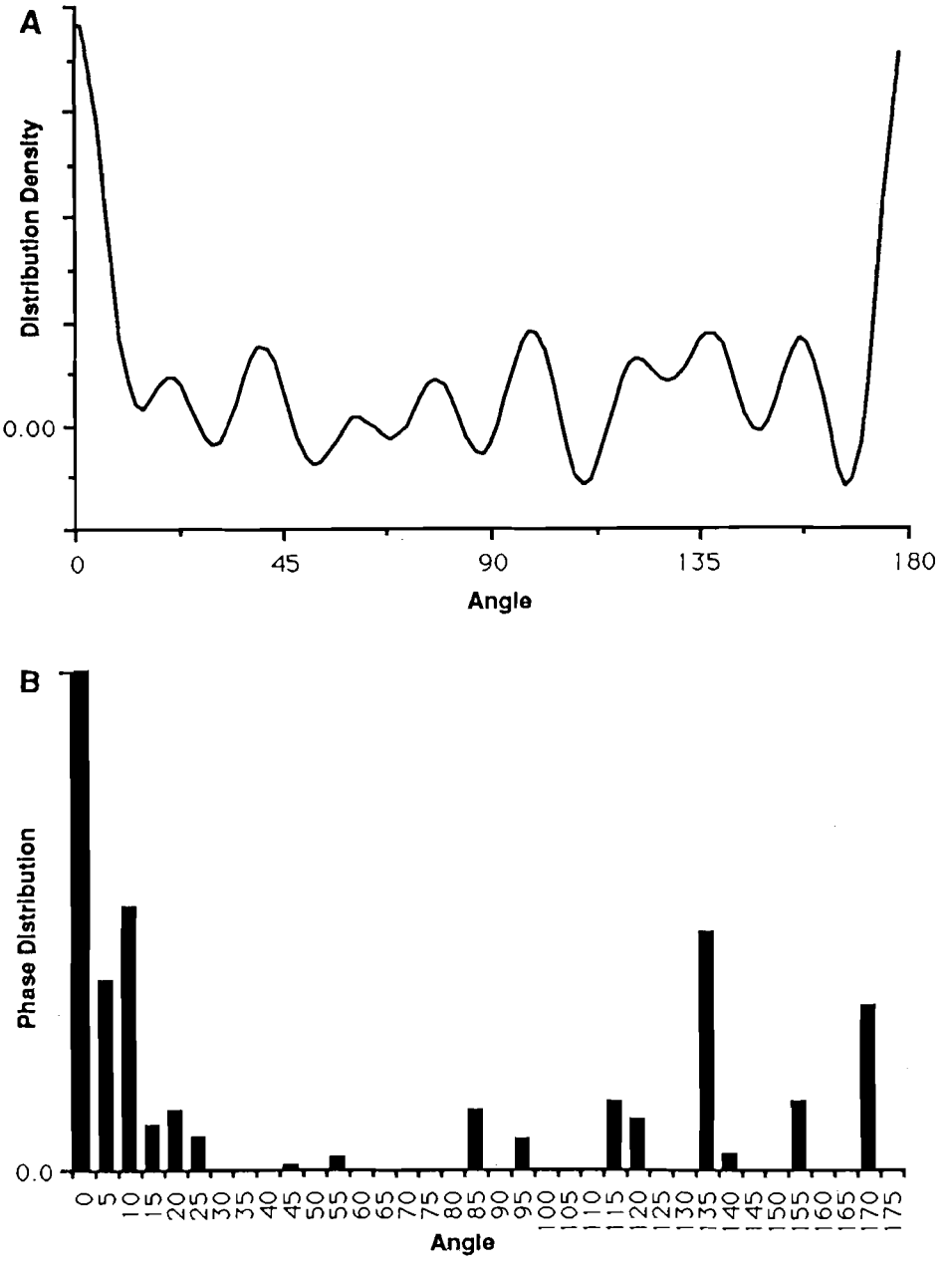

FIG. 4. A: Normalized distribution density plot for sample pattern of Fig. 1. **B:** Normalized phase distribution plot. Both plots are generated using maximum degrees of freedom in the respective procedures. Units are intercepts per unit length.

when testing a typical slice of cancellous bone, because it is difficult to separate noise from data. The inaccuracies are, however, easily illustrated by performing the directed secant method on a digitized circle, shown in Fig. 6A, that theoretically has a circular rose of intercepts, as described in Eq. 15. The rose of intercepts generated by laying test lines 1 pixel in width at each of the angles Θ_i, $i = 1, \ldots, m$ is shown in Fig. 6B, with standard error (esti-

TABLE 1. *Comparison of conventional method with primary direction method for sample pattern of Fig. 1A*

Conventional method		Primary direction method		
Directions	−6.44°, 83.56°	$\phi 1$	0°	(Eq. 17)
Ratio of ellipse axes	2.58:1	$\phi 2$	135°	(Eq. 17)
Orientation	55% (Eq. 2)	$d(\phi 1)$	58%	(Eq. 20b)
r^2	0.98	$d(\phi 2)$	12%	(Eq. 20c)
See (23)		d(isotropy)	30%	(Eq. 20a)
		r^2	0.95	(Eq. 13d)

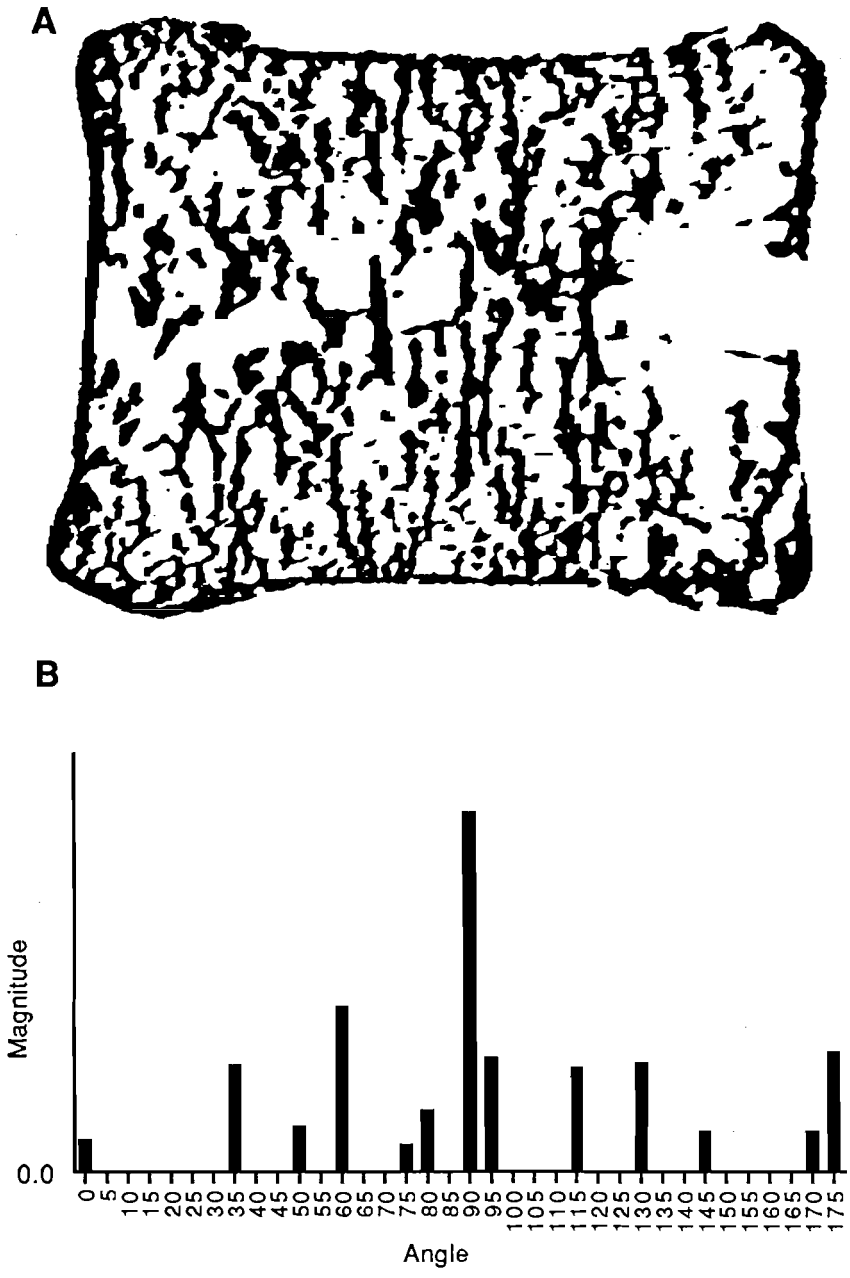

FIG. 5. A: Sagittal section of the second lumbar vertebra in man, from Oxnard and Yang (17) reprinted with permission. **B:** Normalized phase distribution for the section.

mated variance) given. Similarly, the plot generated by rotating the digitized image to each angle within the computer memory is shown in Fig. 6C, also with standard error given. Clearly, both plots exhibit significant departures from the desired result. These variations in results are a result of practical imaging and analysis techniques.

Stereology theory is based on the assumptions that test lines are drawn infinitely thin and that the image is perfectly represented. However, digitized

TABLE 2. *Comparison of conventional method with primary direction method for a sagitally cut human second lumbar vertebra (17)*

Conventional method		Primary direction method		
Directions	−2.45°, 87.55°	$\phi 1$	90°	(Eq. 17)
Ratio of ellipse axes	1.67:1	$\phi 2$	60°	(Eq. 17)
Orientation	36% (Eq. 2)	$d(\phi 1)$	35%	(Eq. 20b)
r^2	0.98	$d(\phi 2)$	4.3%	(Eq. 20c)
See (23)		d(isotropy)	61%	(Eq. 20a)
		r^2	0.98	(Eq. 13d)

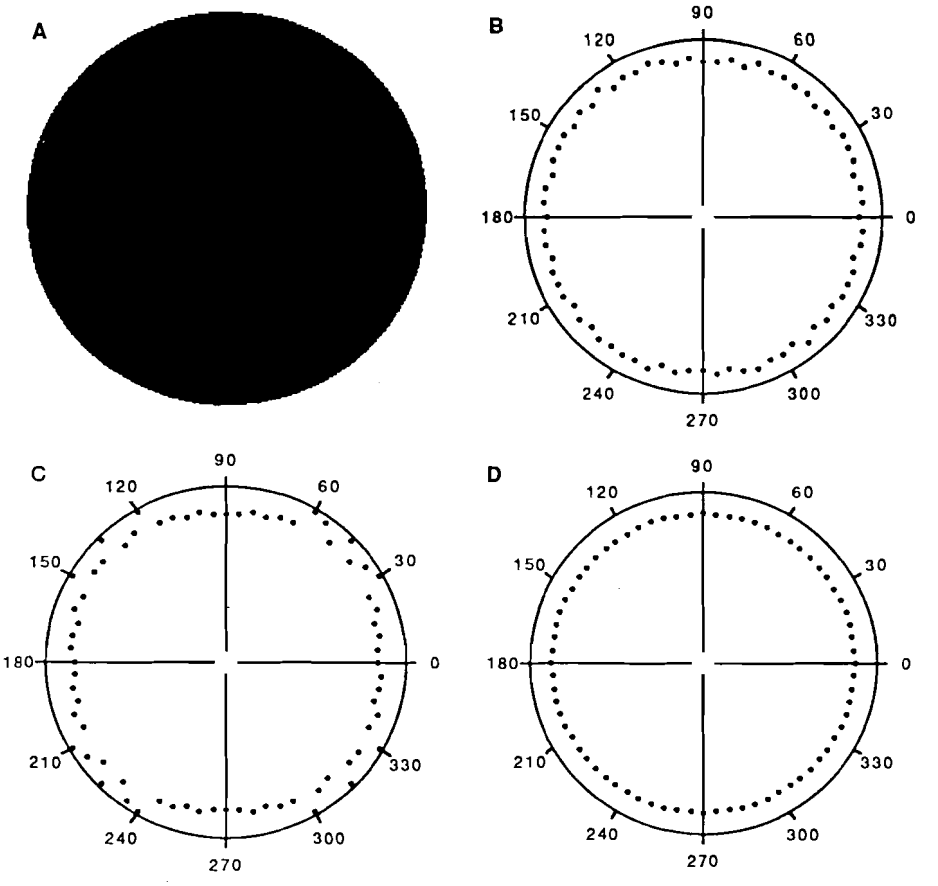

FIG. 6. Accuracy of intercept counts is dependent on stereology technique. **A:** Digitized representation of a circle, which is an isotropic sample pattern. **B:** Corresponding rose of intercepts, with test line width = 1 pixel, produced by rotating test lines. Standard error $s^2 = 4.67 \cdot 10^{-12}$. **C:** Rose of intercepts with test line width = 1 pixel, produced by rotating the image within computer memory. Standard error $s^2 = 2.72 \cdot 10^{-10}$. **D:** Rose of intercepts with test line width = 3 pixels, produced by rotating test lines. Standard error $s^2 = 3.47 \cdot 10^{-15}$.

images with digitized test lines combine to produce an effect of extra intercepts at certain angles. For example, Fig. 7A shows an image and a corresponding test line for a hypothetical image. Theoretically, the stereology computer program should count two intercepts—one each for entering and leaving the substance. However, the digitized test line will actually make six intercepts for the case given. If the stereology computer program always lays test lines horizontally across an image rotated within the computer memory, a similar situation occurs from rounding during the mathematical rotation. Figure 7B shows a hypothetical image that produces an erroneous intercept count when rotated within the computer memory.

There are two remedies to this problem. One is to rotate the specimen physically, redigitizing the image for each angle at which the directed secant method is to be performed. Another, mechanically less complex, remedy is to sacrifice some resolution and lay test lines larger than a single pixel in width. This method calls for counting an intercept only after checking that the pixels across the entire width of a test line have entered a new phase. Applying this method to the circle of Fig. 6A, using test lines ~3 pixels in width, produces a rose of intercepts as shown in Fig. 6D. Note that the standard error is nearly 3 orders of magnitude smaller than that for the conventional technique, as demonstrated in Fig. 6B. A test line width of 3–5 pixels was used to produce the results shown in Figs. 1–5.

Using wide test lines to filter out digitization artifacts can be extended to filter out microstructural features. A substance may have "bumps" or "hairs" that contribute nothing to its structural integrity but produce noise in the rose of intercepts. In some situations, it may be desirable to ignore these small elements. For example, the test substance in Fig. 8A obviously has a single structural direction of orientation. However, it has microstructural features that produce misleading results in the phase distribution, shown in Fig. 8B. If one is interested only in the larger structural features, a test line width larger than the undesirable elements (in this case, 5 pixels wide) can be used to produce the phase distribution shown in Fig. 8C. Note that

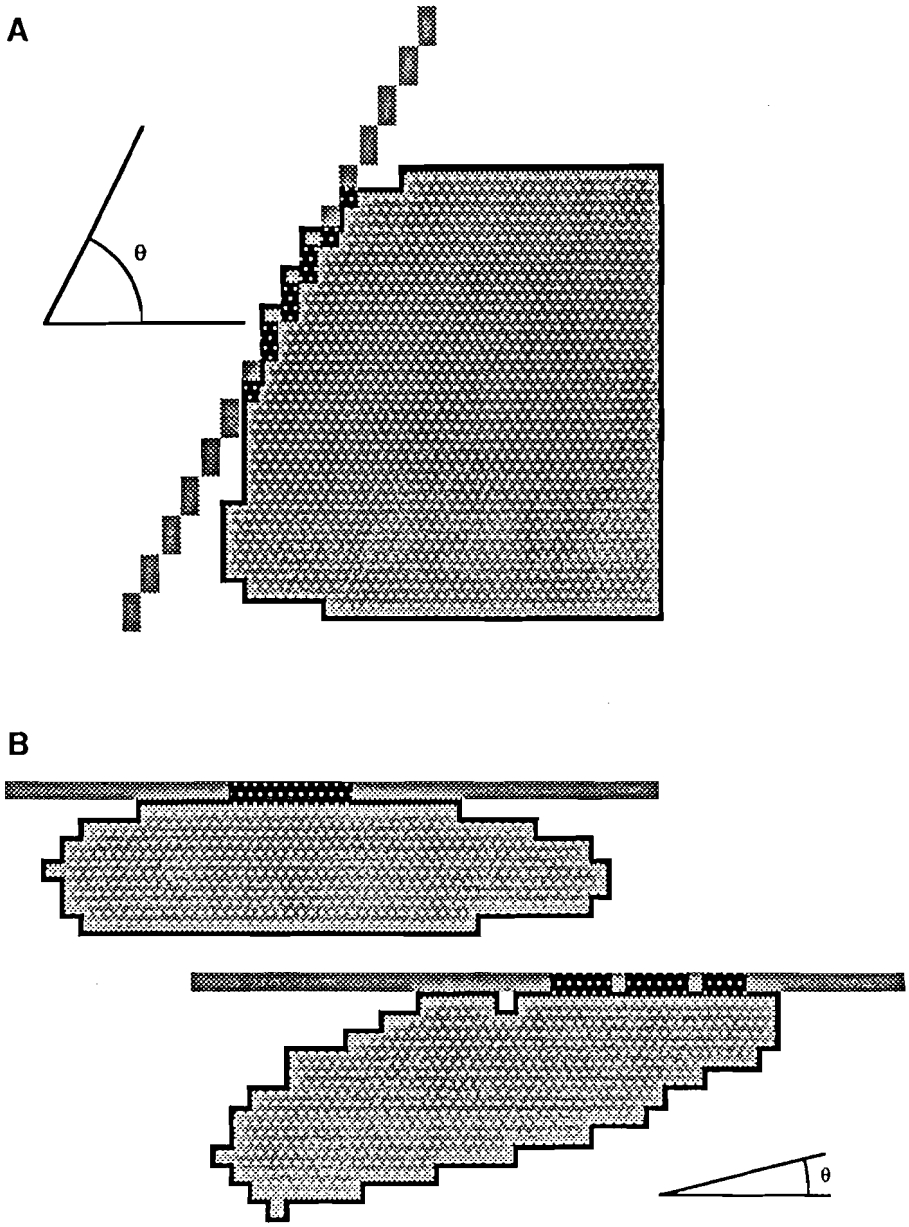

FIG. 7. A: Digitization of an image along with rotation of test lines may result in errors in intercept counts. In this case, there are six intercepts where there should be only two. **B:** Rotation of a digitized image within computer memory, keeping test lines fixed, can also introduce multiple intercept counts. As with (A), this rotation results in six intercepts where there should be only two.

as with all filtering techniques, real data are always difficult to separate from the noise, and the drawbacks and advantages inherent to filtering apply. Of course, other, more traditional smoothing techniques may be applied, but the advantage of this technique is that test line widths may be chosen based on visual inspection of the size of the undesirable elements.

Another consideration when using the directed secant method is the assumption that cancellous bone is a continuum. Harrigan and colleagues (10) showed that this assumption breaks down in various situations in which the control area (or volume) over which the analysis is performed is not sufficiently large relative to the mean intercept length. Harrigan and colleagues suggest that the accuracy of the *MIL* is related to "the inverse of the square root of the number of intercepts measured."

This constraint affects the selection of test line spacing. The spacing should be chosen small enough that a sufficiently large number of intercepts occur over the area to be examined to ensure accuracy, but not smaller than the size of microstructural features, whose intercept counts can signifi-

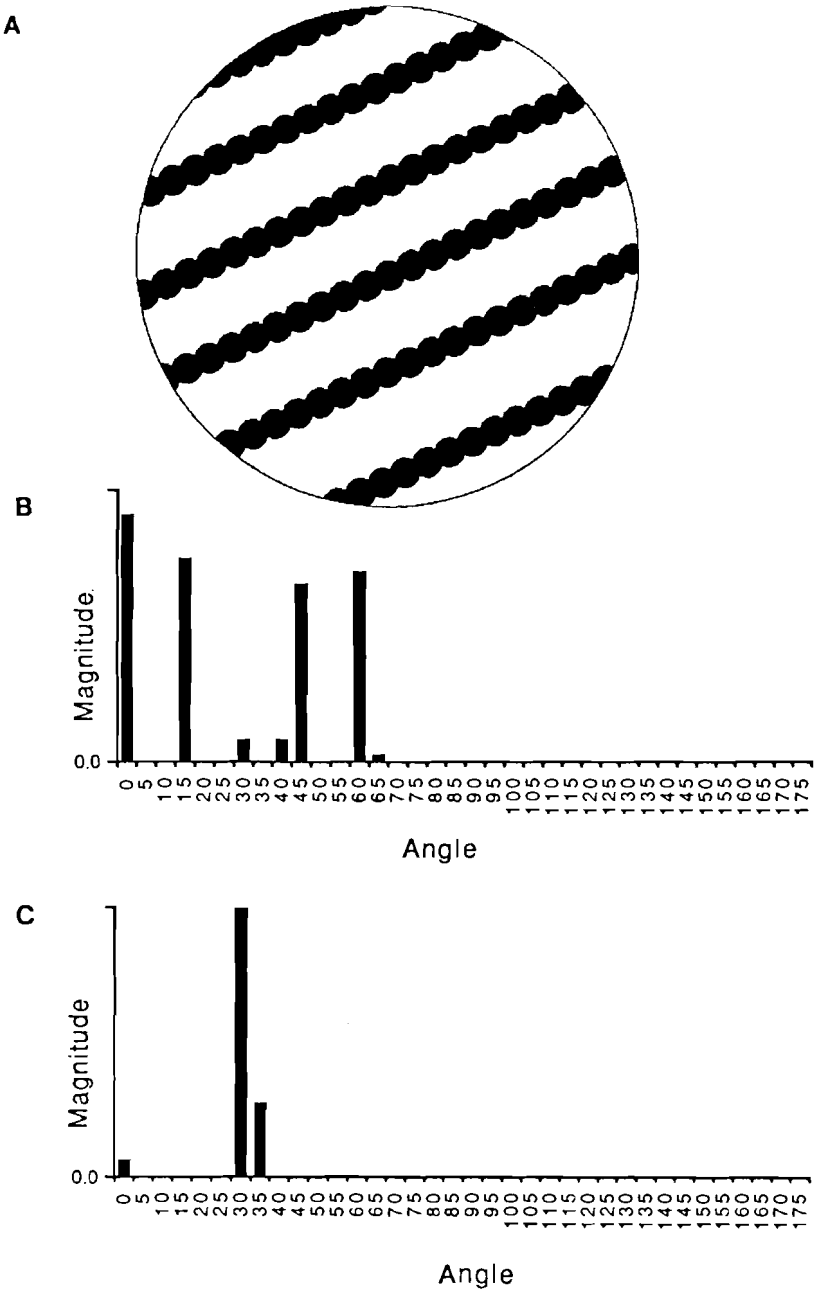

FIG. 8. A: Sample pattern with one structural direction of orientation and microstructural features. **B:** Corresponding normalized phase distribution with test line width = 2 pixels. **C:** Normalized phase distribution with test line width = 5 pixels. Units are intercepts per unit length.

cantly affect the intercept count for the sample. Another trade-off to be kept in mind is that between test line spacing and computational limitations. The smaller the test line spacing, the greater the number of test lines across the sample and, thus, the greater the computational time required to count the intercepts.

A final consideration when analyzing two-dimensional sections of bone to determine orthotropy is whether the plane under study provides relevant information. Since the two-dimensional section provides data only for a plane, one must make certain assumptions to generalize the characterization to three dimensions. Researchers (1,3,11,17, 19,25) have taken care to study sections in the plane of the loading conditions under scrutiny—in effect, assuming a condition such as plane stress or plane strain in the material. It is under similar circumstances that the methods presented here are most applicable.

DISCUSSION

The methods introduced here extend our ability to quantify the orientation of trabecular bone surfaces in a plane. To test the assumption of orthotropy, the phase distribution method should be applied, and the peaks of the plot will signify orthotropy if they are separated by ~90°. The number of large peaks will also denote the number of primary directions present in the substance. The relative magnitudes of the peaks indicate the relative degrees of orientation in the various directions.

If the peaks calculated in the phase distribution method are clustered close together, making it difficult to discern whether the cluster mark separate directions of orientation or simply a broad band of a single orientation, one can assume supposed numbers of directions n and employ the primary direction method. The value of r^2 (Eq. 13d) shows how well the assumption of n directions fits the data.

If the number of directions is estimated, because an assumption is built into a model (or for any other reason), the primary direction method condenses the various extraneous information of the phase distribution method into a best fit for comparison to the model. Together with a measure of the degree of isotropy, the degrees of orientation are more informative than the percentage orientation produced by conventional means.

Accurate intercept measurements can be obtained by careful selection of stereology parameters. Line spacing and width can be chosen to be greater than microstructural features to filter out unwanted data. In addition, the sample area should be small enough to avoid significant variations in orientation across its width yet large enough to satisfy the continuum assumption (10). Proper selection of these parameters will facilitate the production of accurate, informative orientation data.

The phase distribution and primary direction methods, as presented, are appropriate for a properly oriented section of a three-dimensional structure, e.g., a section assumed to undergo plane strain (as used by other researchers working with two-dimensional sections). However, more work is needed to produce a more formal characterization of three-dimensional morphology.

The fundamental question that these methods ideally address is that of the traditional trajectorial theory; that is, are trabeculae aligned orthotropically? This question must be answered before formulations involving *MIL* ellipses or tensors can be used. The methods provide a more precise characterization of the bone architecture and can quantitatively document any deviation from orthotropy present in the bone.

Acknowledgment: Special thanks to J. L. Kuhn and R. W. Goulet for information concerning automated stereology. This research was supported by the National Science Foundation and the Palo Alto Veterans Affairs Rehabitational Research and Development Center.

REFERENCES

1. Bacon GE, Bacon PJ, Griffiths RK: A neutron diffraction study of the bones of the foot. *J Anat* 139:265–273, 1984
2. Carter DR, Orr TE, Fyhrie DP: Relationships between loading history and femoral cancellous bone architecture. *J Biomech* 22:231–244, 1989
3. Cheal EJ, Snyder BD, Nunamaker DM, Hayes WC: Trabecular bone remodeling around smooth and porous implants in an equine patellar model. *J Biomech* 20:1121–1134, 1987
4. Cowin SC: The relationship between the elasticity tensor and the fabric tensor. *Mech Materials* 4:137–147, 1985
5. Cowin SC: Wolff's law of trabecular architecture at remodeling equilibrium. *J Biomech Engineer* 108:83, 1986
6. Devore JL: *Probability and Statistics for Engineers and Scientists,* 2nd. ed. Monterey, CA, Brooks/Cole Publishing Co., 1987
7. Fyhrie DP, Carter DR: A unifying principle relating stress to trabecular bone morphology. *J Orthop Res* 4:304–317, 1986
8. Gill PE, Murray W, Saunders MA, Wright MH: *User's Guide for SOL/QPSOL Version 3.2, Report SOL 84-5,* Department of Operations Research, Stanford University, California, 1984
9. Harrigan T, Mann RW: Characterization of microstructural anisotropy in orthotropic materials using a second rank tensor. *J Materials Sci* 19:761–767, 1984
10. Harrigan TP, Jasty M, Mann RW, Harris WH: Limitations of the continuum assumption in cancellous bone. *J Biomech* 21:269–275, 1988
11. Hayes WC, Snyder B: Toward a quantitative formulation of Wolff's law in trabecular bone. In: *Mechanical Properties of Bone,* ed by SC Cowin, New York, American Society of Mechanical Engineers, 1981, 43–68
12. Hilliard JE: Specification and measurement of microstructural anisotropy. *Trans Met Soc AIME* 224:1201–1211, 1962
13. Kanatani K-I: Procedures for stereological estimation of structural anisotropy. *Intl J Engineer Sci* 23:587–598, 1985
14. Luenberger DG: *Linear and Nonlinear Programming,* 2nd. ed. Rawling, Mass., Addison-Wesley, 1984
15. Meyer GH: Die Architektur der Spongiosa. *Arch Anat Physiol wiss Med* 34:615–628, 1867
16. Murray PDF: *Bones. A Study in the Development and Structure of the Vertebrate Skeleton.* Cambridge, Cambridge University Press, 1936
17. Oxnard CE, Yang HCL: Beyond biometrics: Studies of complex biological patterns. In: Ashton EH, Holmes RL, eds. *Perspectives in primate biology, symposia of the zoological society of London, no. 46.* New York: Academic Press, 1981
18. Philofsky EM, Hilliard JE: On the measurement of the orientation distribution of lineal and areal arrays. *Q Appl Maths* 28:79–86, 1969

19. Raux P, Townsend PR, Miegel R, Rose RM, Radin EL: Trabecular architecture of the human patella. *J Biomech* 8:1–7, 1975
20. Roesler H: The history of some fundamental concepts in bone biomechanics. *J Biomech* 20:1025–1034, 1987
21. Thompson DW: *On Growth and Form,* abridg ed. London, Cambridge University Press, 1917
22. Underwood EE: *Quantitative Stereology,* Reading, MA, Addison-Wesley, 1970
23. Whitehouse WJ: The quantitative morphology of anisotropic trabecular bone. *J Microsc* 101:153–168, 1974
24. Whitehouse WJ: A stereological method for calculating internal surface areas in structures which have become anisotropic as the result of linear expansions or contractions. *J Microsc* 101:169–176, 1974
25. Whitehouse WJ, Dyson ED: Scanning electron microscope studies of trabecular bone in the proximal end of the human femur. *J Anat* 118:417–444, 1974
26. Wolff J: *The Law of Bone Remodeling* (*Das Gesetz der Transformation der Knochen, Hirschwald,* 1892) (Translated by P. Maquet and R. Furlong). Berlin, Springer-Verlag, 1986